Journal of Low Temperature Physics

The Cryogenic AntiCoincidence detector for the ATHENA X-IFU: design aspects by Geant4 simulation, and preliminary characterization of the new single pixel.

--Manuscript Draft--

Manuscript Number:	JLTP-D-15-00265R2
Full Title:	The Cryogenic AntiCoincidence detector for the ATHENA X-IFU: design aspects by Geant4 simulation, and preliminary characterization of the new single pixel.
Article Type:	S.I. : LTD16
Keywords:	TES; Anticoincidence detector; Space; ATHENA
Corresponding Author:	Claudio Macculi INAF/IAPS Roma Roma, Italy ITALY
Corresponding Author Secondary Information:	
Corresponding Author's Institution:	INAF/IAPS Roma
Corresponding Author's Secondary Institution:	
First Author:	Claudio Macculi
First Author Secondary Information:	
Order of Authors:	Claudio Macculi
	Andrea Argan
	Matteo D'Andrea
	Simone Lotti
	Luigi Piro
	Michele Biasotti
	Dario Corsini
	Flavio Gatti
	Angiola Orlando
	Guido Torrioli
Order of Authors Secondary Information:	
Funding Information:	

The Cryogenic AntiCoincidence detector for the ATHENA X-IFU: design aspects by Geant4 simulation, and preliminary characterization of the new single pixel.

C. Macculi [a] • A. Argan [a] • M. D'Andrea [a] • S. Lotti [a] • L. Piro [a] • M. Biasotti [b] • D. Corsini [b] • F. Gatti [b] • A. Orlando [b] • G. Torrioli [c]

[a] INAF/IAPS Roma, Roma, Italy
[b] Genova University, Phys. Dep., Genova, Italy
[c] CNR/IFN Roma, Roma, Italy

Abstract The ATHENA observatory is the second large-class ESA mission, in the context of the Cosmic Vision 2015-2025, scheduled to be launched on 2028 at L2 orbit. One of the two planned focal plane instruments is the X-IFU (X-ray Integral Field Unit), which will be able to perform simultaneous high-grade energy spectroscopy and imaging over the 5 arcmin FoV by means of a kilo-pixel array of transition-edge sensor (TES) microcalorimeters, coupled to a high-quality X-ray optics. The X-IFU sensitivity is degraded by the particle background, induced by primary protons of both solar and Cosmic Rays origin and secondary electrons. A Cryogenic AntiCoincidence (CryoAC) TES-based detector, located < 1 mm below the TES-array, will allow the mission to reach the background level that enables its scientific goals. The CryoAC is a 4-pixels detector made of Silicon absorbers sensed by Iridium TESs. We currently achieve a TRL=3-4 at the single pixel level. We have designed and developed two further prototypes in order to reach TRL = 4. The design of the CryoAC has been also optimized using the Geant4 simulation tool. Here we will describe some results from the Geant4 simulations performed to optimize the design and preliminary test results from the first of the two detectors, 1 cm^2 area, made of 65 Ir TESs.

Keywords TES • Anticoincidence detector • Space • ATHENA

1 From science goals to technologies definition: the need for the CryoAC

The ATHENA (Advanced Telescope for High Energy Astrophysics) [1] will aim at studying some of the most fundamental topics in

contemporary astrophysics and cosmology. One of the on-board instrument is the X-IFU, which is a TES imaging-array. It will provide high spectral energy resolution images in the 0.2-12 keV range with 2.5 eV FWHM. To meet the scientific requirements, in particular for matter assembly in clusters, metal production and dispersal, low surface brightness objects, it is necessary to reduce the background (bkg) in the array down to $5 \cdot 10^{-3}$ cts/cm^2/s/keV. This is possible by adopting an anticoincidence detector called "CryoAC" enabling a primary protons veto efficiency greater than 99.8%, coupled to a secondary electron passive shielding enabling the reduction of this component. For a very brief review about both X-IFU and the CryoAC aspects see [2, 3]. The CryoAC baseline design is based on a thin layer (0.5 mm) Si absorber where the energy deposited by particles is sensed by Ir-TES. The detector located <1 mm below the X-IFU TES array, has an active area of 4.6 cm^2 in 4 pixels, each of ~ 1.15 cm^2, for redundancy/deadtime issues, and a bandpass of 20 keV-0.5MeV. The aim of this paper is to show the progress in the design, development and test of the CryoAC: in §2 we will show an optimization of the CryoAC for maximizing the rejection efficiency by Geant4 simulations; in §3 the development of the last prototypes; in §4 the preliminary test; then the conclusions.

2 GEANT4 simulations impact on the CryoAC-to-X-IFU design

No X-ray detectors have ever flown at L2 orbit, thus to know the particle bkg we estimated it by Monte Carlo simulations, that allowed us also to improve the performances of the CryoAC [4]: see Fig. 1.

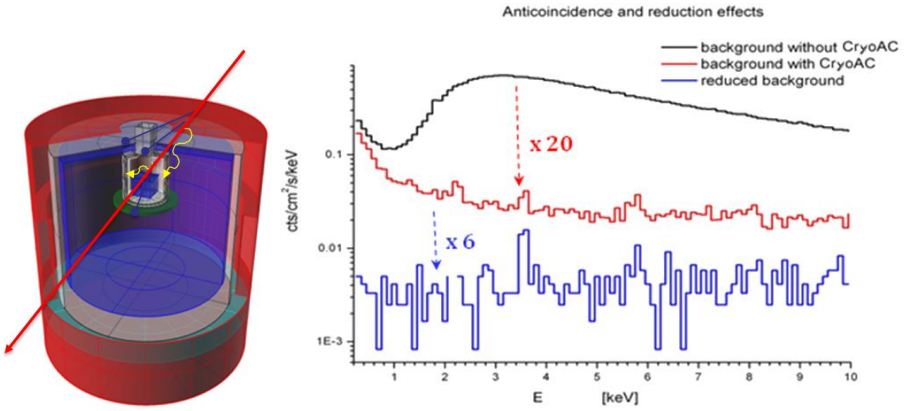

Fig. 1 *Left*: cryostat and focal plane assembly mass model with superimposed particles tracks to emphasize the bkg issue. *Right*: Spectra (100 eV bins) of the bkg expected on X-IFU in several cases. The *black line* is the expected bkg without an anti-coincidence system, the *red line* is the

level expected with the CryoAC, and the *blue line* is the official bkg level ($5 \cdot 10^{-3}$ cts/cm^2/s/keV) using also an electron passive shield. "x20" and "x6" are the reduction factors. (Color figure online).

It can be shown that only primary protons having energies > ~ 150 MeV can reach the Focal Plane Assembly [5]. The number of GCR protons in L2 with energies in the 150 MeV-100 GeV range is about 4.1 pr/cm^2/s [5]. The estimated count rate of protons hitting the TES array at the focal plane and releasing energy below 12 keV is about 3 cts/cm^2/s. We require that the contribution of this component to the background is negligible, i.e. less than 1/10 of the requirement, i.e. less than $5 \cdot 10^{-3}$ cts/cm^2/s/keV. This sets the rejection efficiency to primary GCR > 99.8 %. The rejection efficiency of the system "X-IFU + CryoAC" depends on the geometry (i.e. the size of detector, the size of anticoincidence detector and the distance between them), on the particle energies and on the tracks of these particles in the X-IFU. The geometrical rejection efficiency is the ratio between the number of particles triggering the anticoincidence (CryoAC) after or before hitting the TES array detector (X-IFU) and the number of particles crossing the X-IFU. Further, particle rejection can be increased also considering the following:

1) energy discrimination - if the amount of energy released by particles hitting the X-IFU is above the 12 keV threshold of the instrument the particle can be discriminated.
2) pattern recognition algorithms - unlike the photons for which this event is very unlikely, skew particles can switch-on more than 1 pixel, so allowing the discrimination

The optimization of the CryoAC for maximizing the rejection efficiency was performed with the Geant4 simulations toolkit by taking into account the geometry of the "X-IFU and CryoAC" system. We have investigated how the size of the CryoAC and its distance from the microcalorimeter array influences the rejection efficiency, also taking into account both energy discrimination and pattern recognition algorithms: this provides what we call the effective rejection efficiency. We decided first to fix the ratio of the sizes of the CryoAC and of the main detector, R, and found out that the rejection efficiency increases as the CryoAC is placed closer to the main TES array (see Fig. 2-left). Afterwards we fixed the distance at the minimum possible value, i.e. 1 mm, and investigated how the ratio R of the CryoAC linear size relative to the X-IFU one influences the rejection efficiency (see Fig. 2-right and Ref. 6).

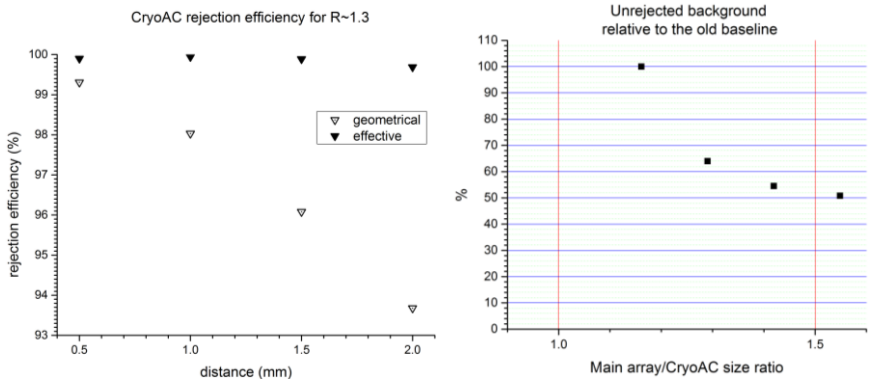

Fig. 2 - *Left*: geometrical and effective rejection efficiency of the CryoAC relative to the linear size ratio R~1.3 as function of the CryoAC distance from the microcalorimeter array. *Right*: percentage of the un-rejected particle background at distance d = 1 mm referred to the old baseline CryoAC design (i.e. the CryoAC size foreseen before this study) versus the main array-to-CryoAC sizes ratio.

Summarizing, we have found as expected that for high CryoAC efficiencies, small distances and large sizes are necessary. There is, however, a tradeoff between these requirements and the mechanical and manufacturing constraints for this detector. The minimum distance at which the detector can be actually mounted is about 1 mm, that fixes the ratio R between the linear sizes of the CryoAC and microcalorimeter array to about 1.3. In the future perspective of the X-IFU final design with an hexagonal shape and a side of ~1 cm, the CryoAC detector should be upgraded to have the same shape and a bit larger size, corresponding to a total area of about 4.6 cm^2, divided among 4 trapezoidal pixels of ~1.15 cm^2. Further increase of size adds more problems to the manufacturing process without commensurable benefits.

3 Development of the last prototypes: AC-S7, AC-S8

Two new prototypes of the CryoAC pixels were produced from the same Silicon wafer at the Genova University (Phys. Dept.), namely AC-S7 and AC-S8, (Fig. 3). The TES sensing structure is made of 65 uniformly distributed, 100x100 μm^2 wide and 200 nm thick, Ir films grown with Pulsed Laser Deposition. The TES are parallel connected through Nb lines deposited with RF sputtering. These features have been proven to be the best compromise among the large and uniform surface coverage for an efficient athermal signal detection and the necessity of constraining down the heat capacity contribution of the metal films. One of the prototypes, ACS-8, has

in addition different Al-fingers directly connected to the TES to investigate the feasibility of a further efficiency improvement [7, 8, 9].

The athermal phonons are produced in the downgrading of the primary energy released by the cosmic particles in silicon and contributes for few percents to the signal area. At sub-Kelvin regime, this has been found as the first observable and quick transfer of energy from the particle tracks to the sensors [10]. Therefore, we have enhanced the TES sensor efficiency to this tiny signal in order to speed-up the response rise-time of such a large detector, important feature for an anticoincidence detector.

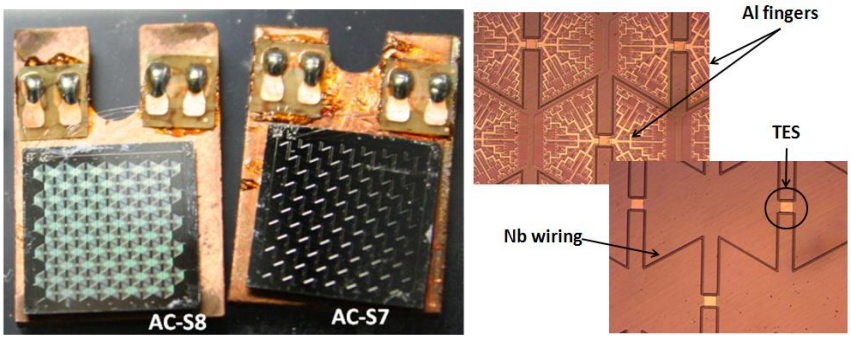

Fig. 3 *Left*: the AC-S8 and AC-S7 samples. *Right*: details about the TES, Nb wiring and Al-fingers. (Color figure online).

In the next Table 1 we report the main characteristics of the samples:

Absorber Silicon size:	10x10 mm^2, 380 μm thick
TES (x 65) Iridium size:	100x100 μm^2, ~ 200 nm thick
Niobium wiring:	~ 870 nm thick
Silicon wafer	5-10 Ω·cm

Tab 1 Main parameters of the produced samples.

4 Preliminary characterization of the AC-S7 prototype.

We describe here the preliminary characterization of the AC-S7 prototype from the reported measurements: the TES transition curve

acquired in 2 different laboratories (Genova and Roma), and the preliminary test performed at Genova by illuminating the detector by a ^{241}Am source.

4.1 The transition curve

In Fig. 4 are shown the transition curves that have been measured with two different setups and readout techniques: blue data - Genova Univ. laboratory (dilution refrigerator, 4-wires technique with Lock-in amplifier), red-data INAF laboratory (ADR, SQuID, modulation technique sine-wave at 22Hz). The plot shows a transition width from 10% to 90% of about 2 mK and a temperature shift of the central value of 2.7 mK, that is within the presently absolute temperature calibration uncertainties among the two cryogenic systems. The normal resistance is about 1.4 mΩ and shows very small deviations within the errors. The gamma parameters are consistent well below 2σ errors. We consider this comparison a good reproducibility test of the transition curve measurement performed by different techniques and a demonstration that the Genova laboratory manufacturing processes of these large area samples are well consolidated and stable.

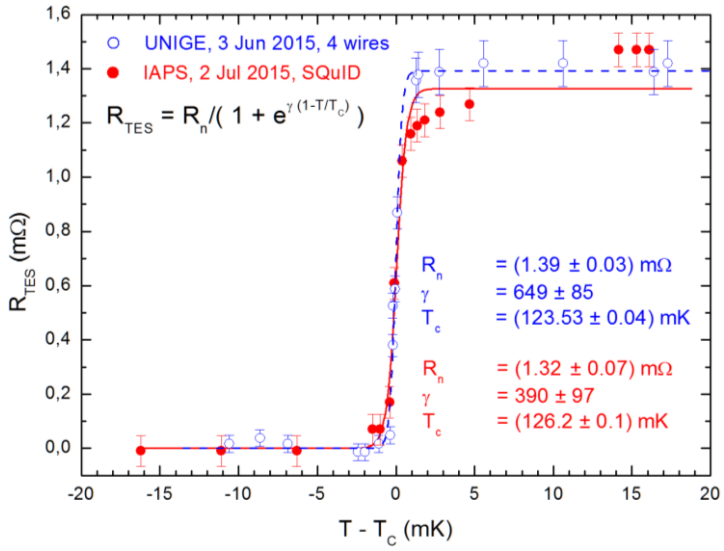

Fig. 4 Comparison between the two transition curves measured at Genova and Roma laboratories. The temperature data error is < 100 μKpp, not visible in this picture. The error bars related to the IAPS resistance data have been assessed by evaluating the contribution from the shunt resistor, the bias current and the feedback voltage. The error bars related to the UniGe data come directly from the lock-in acquisition. Gamma is a fitting parameter

related to the α one evaluated at the critical temperature T_C: $\gamma = 2 \cdot \alpha$. Please note that here it is $R(T_C) = R_N/2$. (Color figure online).

4.2 Illumination by the 60 keV line from ^{241}Am

The response to radiation excitation and the preliminary analysis were done by illuminating the AC-S7 with an ^{241}Am source. The source was preliminary shielded in order to filter out the fluorescence lines. The setup has been tested at room temperature with a Canberra Germanium detector for evaluating in detail the expected count rate in AC-S7 and the absence of unwanted lines. The typical acquired pulses are shown in Fig. 5.

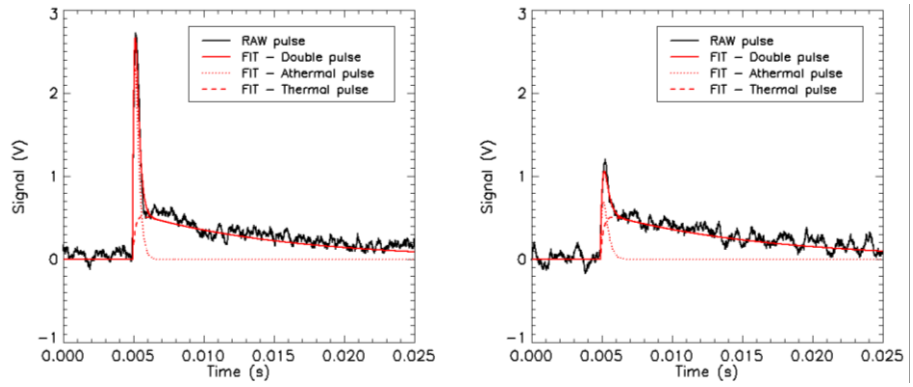

Fig. 5 AC-S7 raw pulses: it is evident the fast athermal component and the slow thermal one. The acquisition time has been about 2 hours. (Color figure online).

The pulses show clearly both the fast athermal and the slow thermal components, as expected for Silicon. A rough result from the double pulse fitting procedure [3, 10] is overplotted just to provide a view about the fast athermal component and the slow thermal one: the work is under way to investigate deeply this dynamics. We have performed the in-time integration of the acquired pulses after subtracting the averaged and extrapolated baseline from the pre-triggered data stream. As well known the distribution of these values is proportional to the released energy. The in-time integral histogram shows a well shaped spectrum and the expected 60 keV line is evident (Fig. 6). It is further possible to roughly evaluate a threshold of about 20 keV consistent with our requirements [3]. The analysis don't include the optimal signal filtering and the line width is the genuine results of the simple in-time integration. Then line-width include effects of the baseline fluctuations, un-rejected in-band noise and probably the

composition of all the effects of a second order not uniformity in such a large detector based on 65 TESs. Further work is under way to investigate deeply these issues.

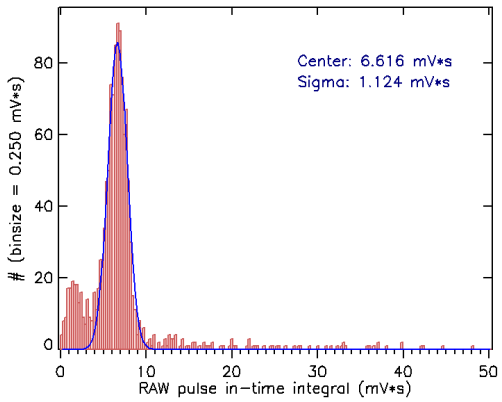

Fig. 6 AC-S7 data pulse in-time integral: raw analysis. A gaussian fit on the main line is overplotted. (Color figure online).

5 Conclusions

The TES-based CryoAC detector is fundamental to enable part of the ATHENA science goal by reducing the residual particle background: its development is framed into the one of the X-IFU instrument. The Geant4 toolkit has been used to design the CryoAC in order to get the science goals: our final design foresees 4 pixels for a full active area of 4.6 cm^2 area.

We have produced 2 new single pixel prototypes: wide area (1 cm^2), with (AC-S8) and without (AC-S7) Al-fingers. They are featured by 65 Ir TES deposited onto Silicon absorber. The AC-S7 transition curve measurement (Fig. 4) performed at different laboratories, by different techniques and refrigerators is consistent: this result consolidates the manufacturing processes.

We have illuminated the AC-S7 pixel by the ^{241}Am-60 keV line to test its response, mainly to understand how the TES network works in collecting the athermal phonons. The preliminary results show the expected well shaped 60 keV line (Fig. 6), and it is possible to roughly evaluate a threshold of about 20 keV consistent with our requirements.

Acknowledgements
This work has been performed under the ASI contract 2014-045-R.0.

References

Title

1. http://athena2.irap.omp.eu/spip.php?rubrique10/
2. L. Ravera, D. Barret, J.W. den Herder, L. Piro, et al., Proc. SPIE **9144**, 91442L (2014); doi: 10.1117/12.2055884
3. C. Macculi, L. Piro, et al., Proc. SPIE **9144**, 91445S (2014); doi: 10.1117/12.2054946
4. S. Lotti et al., Astronomy and Astrophysics, **A54**, 569, (2014)
5. S. Lotti et al., Nuclear Instruments and Methods in Physics Research Section A, **686**, 31, (2012)
6. S. Lotti et al., Proc. SPIE, **9144**, 91442O, (2014).
7. C. Macculi et al., J Low Temp Phys, **167**, 783, (2012)
8. Pizzigoni G. et al., Journal of Physics: Conference Series, **507**, 042031, (2014)
9. C.N. Bailey et al., J. Low Temp. Phys., **167**, 236 (2012)
10. F. Pröbst et al., J. Low Temp. Phys. **100**, (1995)